Journal of Materials Chemistry A

Accepted Manuscript

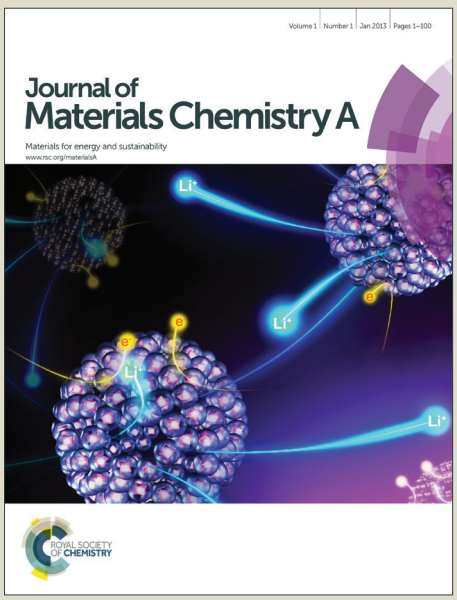

ROYAL SOCIETY OF CHEMISTRY

www.rsc.org/materialsA

Journal of Materials Chemistry A

Cite this: DOI: 10.1039/c0xx00000x

www.rsc.org/xxxxxx

Full Paper

Supercritical Solvothermal Preparation of $Zn_xCd_{1-x}S$ Visible Photocatalyst with Enhanced Activity†

Jiahui Zhong, Ya Zhang, Changqun Hu, Rujing Hou, Haibo Yin, Hexing Li, and Yuning Huo*

Received (in XXX, XXX) Xth XXXXXXXXX 20XX, Accepted Xth XXXXXXXXX 20XX
DOI: 10.1039/b000000x

Ternary $Zn_xCd_{1-x}S$ solid solution was prepared by supercritical solvothermal route and used as photocatalyst without further thermal treatments. This $Zn_xCd_{1-x}S$ exhibited high activity in photocatalytic degradation of rhodamine B and *p*-chlorophenol under visible light irradiation owing to the uniform crystal growth with well-distributed crystallite size, the high specific surface area with large pore volume, and the low recombination rate of photo-induced electrons and holes. Meanwhile, the $Zn_xCd_{1-x}S$ solid solution displayed strong stability against either the structural damage or the oxidation, leading to the excellent durability in photocatalysis.

1. Introduction

Photocatalysis has attracted more attentions due to its potential applications for solving environmental problems and realizing solar energy conversion.[1, 2] Since TiO_2 is limited in the practical application under visible light irradiations due to the wide band gap (E_g = 3.2 eV), considerable efforts for modifying TiO_2 and developing non-TiO_2 photocatalysts have been attempted to extend the light absorption to the visible light region in the past decades.[3-6] Among these active photocatalysts, metal sulfide based materials are powerful for the light harvesting semiconductors and are also the efficient co-catalysts to promote charge separation and to provide active reaction sites. Meanwhile, the heterojunction semiconductor has been used as a building block for nanodevices owing to its unique properties.[7] For example, the H_2 evolution property of MoS_2/CdS catalysts is enormously increased by loading MoS_2 as a cocatalyst, indicative of the crucial effect of the intimate contact between CdS and MoS_2 for the inter-electron transfer between two components.[8, 9] The MoS_2 can also inhibit the photo-corrosion of CdS efficiently.[10] The nanostructured MoS_2 grown on graphene sheets exhibits excellent H_2 evolution photoactivity owing to the high exposure of the MoS_2 edges and the strong electronic coupling to the underlying planar support.[11] The heterojunction of carbon nitride (CN) and sulfur-mediated CN (CNS) can drive the migration of photo-generated electrons from CN to CNS.[12] The CdS-ZnS heterojunction also enhances their photocatalytic activity by interfacial charge transfer and the photo-corrosion of CdS is minimized by dispersing CdS on the surface of ZnS.[13, 14] The key point for the CdS-ZnS heterojunction is to achieve the strong combination between CdS and ZnS and the uniform distribution of each material. The formation of solid solution is possibly an efficient and feasible way for the strong combination and the uniform dispersion of different atoms, greatly beneficial for the separation of photo-induced charges. Ternary chalcogenide nanocrystals, such as $Zn_xCd_{1-x}S$ solid solutions, have also received more attention because the composition-dependent band gap engineering offers new opportunities to harvest visible-light energy.[15-18] More importantly, $Zn_xCd_{1-x}S$ solid solutions keep the transport property of free charges in its perfect crystals and prevent the recombination of photo-induced holes and electrons due to the possibility of forming electrostatic field.[19, 20] Meanwhile, it is also a powerful way to inhibit the

The Education Ministry Key Lab of Resource Chemistry, Shanghai Key Laboratory of Rare Earth Functional Materials, Shanghai Normal University, Shanghai 200234, China. E-mail: huoyuning@shnu.edu.cn; Fax: 86-21-6432-2272; Tel: 86-21-6432-1673.

† Electronic supplementary information (ESI) available: TG-DTA curve of $Zn_{0.21}Cd_{0.79}S$ sample (Fig. S1), Linear relationship of the lattice parameter (a) of $Zn_xCd_{1-x}S$ as a function of X value (Fig. S2), TEM and HRTEM images of (a) ZnS and (b) CdS catalysts (Fig. S3), N_2 adsorption-desorption isotherm and pore size distribution (insert) of $Zn_{0.21}Cd_{0.79}S$ sample (Fig. S4), Variation of E_g with X value (Fig. S5), PL spectra of different samples (Fig. S6), Photocurrent response tests of different samples under visible light irradiation (Fig. S7), RhB photocatalytic degradation on $Zn_{0.21}Cd_{0.79}S$ and 0.21ZnS-0.79CdS(M) (Fig. S8), RhB photocatalytic degradation on $Zn_{0.21}Cd_{0.79}S$ samples obtained at different solvothermal temperature (Fig. S9), 4-CP photocatalytic degradation on different samples (Fig. S10) and XRD patterns of $Zn_{0.21}Cd_{0.79}S$ photocatalyst after each photocatalytic reaction cycle (Fig. S11). See DOI: 10.1039/c0xx00000x

photo-corrosion of CdS *via* the oxidization effect of photo-generated holes[4, 21] during the photocatalytic reaction.

Although $Zn_xCd_{1-x}S$ solid solutions have been prepared by a variety of techniques including solid state reaction[22], cation-exchange reactions[23], microwave synthesis[24], self-assembly approach[25], and hydrothermal process[19, 26], it is still in need of exploring the novel preparation process to obtain $Zn_xCd_{1-x}S$ solid solutions with high photocatalytic activity and stability, as well as the high yield *via* flexible reaction conditions and short reaction time. Supercritical solvothermal process has been considered as an efficient synthesis method for the preparation of metal compounds with nanostructures. It provides the powerful way for the controllable nano-structures within short reaction time and without any further high-temperature heat treatments[27] and maintains the nano-scale architecture during the removal of the solvent.[28] More importantly, the supercritical fluid encourages the high crystal nucleation rates with little subsequent crystal growth leading to the very small particles.[29-31] It is mainly resulted from the unique properties of supercritical fluid including gas-like diffusivity and zero surface tension, and the low viscosity of the reactants in the supercritical fluid.[32-34]

Herein, we successfully synthesized the ternary $Zn_xCd_{1-x}S$ photocatalyst with tunable chemical composition *via* the supercritical solvothermal method in ethanol fluid without any post-thermal treatment. The $Zn_xCd_{1-x}S$ nanospheres were formed by the well-dispersed nanoparticles through the controllable crystal growth in supercritical fluid. Additionally, the strong combination of different atoms in $Zn_xCd_{1-x}S$ was greatly beneficial for the separation of photo-induced charges, leading to the enhanced photocatalytic activity and strong durability.

2. Experimental details

2.1 Synthesis of $Zn_xCd_{1-x}S$ photocatalysts

$Zn_xCd_{1-x}S$ samples were synthesized following the supercritical solvothermal route. Desired molar ratios of $Cd(Ac)_2{\cdot}2H_2O$ and $Zn(Ac)_2{\cdot}2H_2O$ with the total 1.0×10^{-3} mol of Cd^{2+} and Zn^{2+} were first dissolved in a beaker with 30 ml absolute ethanol, and then 4.0×10^{-3} mol CH_3CSNH_2 was rapidly added into the above beaker. After stirring at 25 °C for 15 min, the precursor solution was transferred into a 500 ml autoclave containing 170 ml absolute ethanol solution and was heated to 245 °C at the speed of 4 °C/min. The pressure was kept at 6.5 MPa to reach the ethanol supercritical point (243 °C and 6.4 MPa). After being treated under this supercritical condition for 10 min, the system was allowed to cool slowly to room temperature naturally. Then, the precipitate was centrifuged, washed with distilled water and ethanol for 3 times, and dried at 80 °C for 12 h. The obtained samples were denoted as $Zn_xCd_{1-x}S$ ($0 \le X \le 1$), in which X value represented the molar ratio of Zn atom in the catalysts. For comparison, the mono-dispersed mesoporous $Zn_{0.21}Cd_{0.79}S$(R) sample was prepared via self-assembly approach according to the previous report.[25] The mechanical mixture of pure ZnS (X = 1.0) and CdS (X = 0.0) with the same Zn/Cd molar ratio as that in $Zn_{0.21}Cd_{0.79}S$ was denoted as 0.21ZnS-0.79CdS(M).

2.2 Characterization

The structure of catalysts was determined by X-ray diffraction (XRD) patterns on Rigacu Dmax-3C (Cu Kα radiation). The crystallite size was calculated based on the Scherrer equation ($D = K\lambda/\beta\cos\theta$). The morphologies of the materials were observed and analyzed by transmission electronic micrograph (TEM) on a JEM-2010. The N_2 adsorption-desorption isotherms were obtained on a NOVA 4000 at 77 K, from which the specific surface area (S_{BET}), pore volume (V_P), and average pore diameter (D_P) were calculated by using BJH method. The thermogravimetric and differential thermal analysis (TG-DTA) curves were recorded on a TGA, DTG-60H instrument at a heating rate of 10 °C/min using α-Al_2O_3 as the standard material in air. UV-visible diffuse reflectance spectra (UV-vis DRS) and photoluminescence spectra (PLS) were conducted on MC-2530 and Varian Cary-Eclipse 500, respectively. The band gap (E_g) was calculated based on $ahv = A(hv - E_g)^n$, where a, v, A and n were the absorption coefficient, the light frequency, a constant and 1.0, respectively.[35] The X-ray photoelectron spectroscopy (XPS) analysis was performed on a Perkin-Elmer PHI 5000C. All the binding energies were calibrated by using the contaminant carbon (C_{1S}, 284.6 eV) as a reference. The metal ion concentrations were determined by using inductively coupled plasmatomic emission spectroscopy (ICP, VISTA-MPX). Photocurrent measurement was carried out on a CHI electrochemical analyzer (CHI 660D) in a standard three-electrode configuration with 0.2 mol/L Na_2SO_4 electrolyte. The catalyst coated on the substrate of ITO conductive glass was used as the photoanode (surface area = 4.0 cm^2), while a Pt foil and a saturated calomel electrode (SCE) were used as the counter electrode and the reference electrode, respectively. A 300 W Xe lamp was used as the light source with the distance of 10 cm to the surface of photoanode. The lights with wavelength less than 400 nm were removed by a glass filter (JB-400). Electrochemical impedance spectroscopy (EIS) was performed using an electrochemistry workstation (BAS Epsilon). Experiments were carried out on the film sample in 0.3 M $LiClO_4$ solution (pH = 3) at 1000 Hz with the saturated calomel electrode (SCE) as the reference electrode and Pt as the counter electrode. The Mott-Schottky (M-S) plots were measured to evaluate the flat-band potential following the linear variation of electric capacity (C_{SC}^{-2}) with respect to the applied potential (E) (Eq. 1). N_D and ε represented the doping density and dielectric constant of the prepared samples, respectively.[36] Then, the flat-band potential (E_{fb}) could be confirmed according to the x intercept.

$$C_{SC}^{-2} = (1.41\times10^{20} / N_D\varepsilon)[E - E_{fb} - 0.026] \qquad (1)$$

2.3 Photoactivity test

The liquid-phase photocatalytic degradations of 50 mL 10 mg/L rhodamine B (RhB) and *p*-chlorophenol (4-CP) were carried out at 30 °C in one 100 mL self-designed quartz photochemical reactor containing 25 mg and 50 mg photocatalyst, respectively. After being vigorously stirred for 1 h to reach the adsorption-desorption equilibrium, the photocatalytic reaction was initiated by irradiating the system with one 300 W xenon lamp located at 30 cm above from the reaction solution. All the UV lights with the wavelength less than 420 nm were cut off by a glass filter. At given time intervals, the concentrations of RhB and 4-CP were analyzed by a UV spectrophotometer (UV 7504/PC) at their characteristic wavelengths (λ_{RhB} = 553 nm, $\lambda_{4\text{-}CP}$ = 224 nm) to determine the degradation rate. Preliminary tests demonstrated a good linear relationship between the light absorbance and the pollutants concentration. Only less than 5% RhB and 4-CP decomposed after reaction for 2 and 4 h, respectively, in the absence of either the catalyst or the light irradiation. It could be neglected in comparison to the phtotcatalytic degradation process. The reproducibility was checked by repeating the results at least three times and was found to be within acceptable limits (±5%). The durability of the catalysts was measured according to the following procedure. After each run of RhB photocatalytic degradation, the catalysts were centrifuged and washed with distilled water for 3 times and dried at 100 °C for 12 h. Each

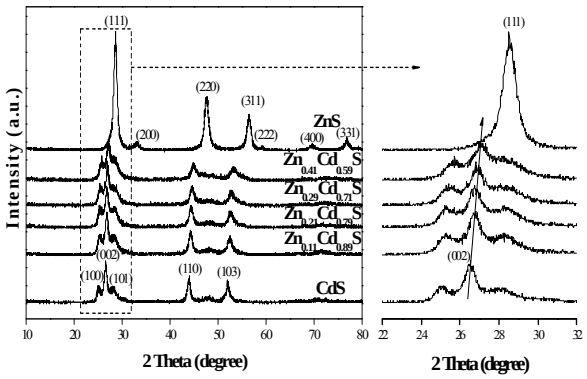

Fig. 1 XRD patterns of different samples with the enlarged patterns.

recycling test was conducted under the same conditions for 2 h and the RhB photodegradation rate was determined to show the change of activity.

3. Results and discussion

Supercritical solvothermal route could realize the high reaction rate and high yield of metal compounds without subsequent high-temperature heat treatments. During the supercritical solvothermal process, desired molar ratios of $Cd(Ac)_2{\cdot}2H_2O$ and $Zn(Ac)_2{\cdot}2H_2O$ reacted with excess CH_3CSNH_2, leading to the formation of $Zn_xCd_{1-x}S$ particles possibly as the following reactions (Eq. 2-5). The yield of $Zn_xCd_{1-x}S$ catalysts was high up to about 87%.

$$Cd(Ac)_2{\cdot}2H_2O \rightarrow CdO \quad (2)$$

$$Zn(Ac)_2{\cdot}2H_2O \rightarrow ZnO \quad (3)$$

$$CH_3CSNH_2 \rightarrow H_2S + CH_3CN \quad (4)$$

$$X\,ZnO + (1\text{-}X)\,CdO + H_2S \rightarrow Zn_xCd_{1-x}S + H_2O \quad (5)$$

According to the ICP results, the actual concentrations of Cd and Zn atoms in the catalyst were similar to the theoretical concentration. TG-DTA curve in Fig. S1 revealed the organic residues in catalyst were removed completely and the catalyst was thermally stable since the weight loss was less than 3.0% without any corresponding endothermal peak below 560 °C. The increased weight above 560 °C and the corresponding exothermal peak at 580 °C were possibly owing to the oxidation of $Zn_{0.21}Cd_{0.79}S$. Fig. 1 showed the XRD patterns of all $Zn_xCd_{1-x}S$ samples with tunable metal contents prepared *via* supercritical solvothermal method. With the increase of X value, it could be found that

Table 1 Structure parameters and band gap of $Zn_xCd_{1-x}S$ samples.

Sample	S_{BET} ($m^2.g^{-1}$)	V_p ($cm^3.g^{-1}$)	D_p (nm)	$D_{Crystallite}$ (nm)	E_g (eV)
CdS	47	0.12	9.4	16	2.2
$Zn_{0.04}Cd_{0.96}S$	43	0.12	9.4	15	2.2
$Zn_{0.11}Cd_{0.89}S$	44	0.13	9.5	15	2.3
$Zn_{0.21}Cd_{0.79}S$	55	0.15	9.5	15	2.3
$Zn_{0.29}Cd_{0.71}S$	58	0.16	9.5	15	2.4
$Zn_{0.41}Cd_{0.59}S$	60	0.16	9.5	14	2.5
ZnS	148	0.21	3.6	12	3.4

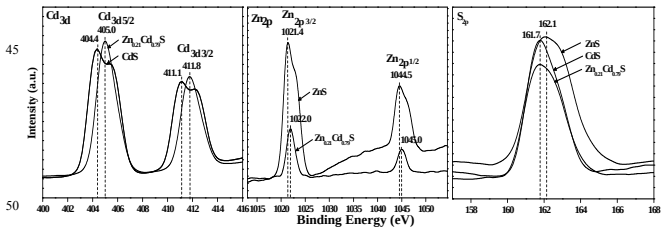

Fig. 2 XPS spectra of $Zn_{0.21}Cd_{0.79}S$, CdS and ZnS samples.

the diffraction peaks of $Zn_xCd_{1-x}S$ ($0 < X < 1$) gradually moved to the larger angles with the shift of about 0.6°, indicating that the obtained nanocrystals were existed in the state of solid solutions rather than the mechanical mixture of CdS (JCPDS 41-1049) and ZnS (JCPDS 65-0309).[37, 38] At the same time, the shift could be attributed to the volume deformation and decrease of unit cell size with the incorporation of Zn atom in $Zn_xCd_{1-x}S$, since Zn^{2+} had a smaller atomic size (0.74 Å) than Cd^{2+} (0.97 Å) [18, 24], resulting in the gradually decreased crystallite size (see Table 1). The lattice parameter (a) of $Zn_xCd_{1-x}S$ presented the linear relationship with the X value (Fig. S2), which followed the Végard's Law and implied the strong electronic effects in the solid solution. [37, 39]

From Fig. 2, XPS spectra further confirmed the formation of solid solutions. The binding energy of Cd_{3d} including $Cd_{3d3/2}$ at 411.8 eV and $Cd_{3d5/2}$ at 405.0 eV in $Zn_{0.21}Cd_{0.79}S$ was higher than that of pure CdS with $Cd_{3d3/2}$ at 411.1 eV and $Cd_{3d5/2}$ at 404.4 eV. Additionally, the binding energy of Zn 2p involving $Zn_{2p1/2}$ at 1045.0 eV and $Zn_{2p3/2}$ at 1022.0 eV in $Zn_{0.21}Cd_{0.79}S$ was higher than that of pure ZnS with $Zn_{2p1/2}$ at 1044.5 eV and $Zn_{2p3/2}$ at 1021.4 eV.[38] Otherwise, the binding energy of S_{2p} at 161.7 eV in $Zn_{0.21}Cd_{0.79}S$ was lower than that of ZnS (162.1 eV) but very close to that of CdS (161.7 eV). The significant shift of binding energy in $Zn_{0.21}Cd_{0.79}S$ comparing to both ZnS and CdS implied the formation of solid solutions. It was resulted from the electron transfer from both Zn and Cd to S atom in $Zn_{0.21}Cd_{0.79}S$, since the strong combination between different atoms in $Zn_{0.21}Cd_{0.79}S$ realized the easy electron transfer. The binding energy of S_{2p} in $Zn_{0.21}Cd_{0.79}S$ close to that of CdS was owing to the dominant content of Cd atom in $Zn_{0.21}Cd_{0.79}S$ catalyst.

The morphology of $Zn_{0.21}Cd_{0.79}S$ photocatalyst shown in TEM images (Fig. 3) presented the shape of sponge-like nanospheres with the average

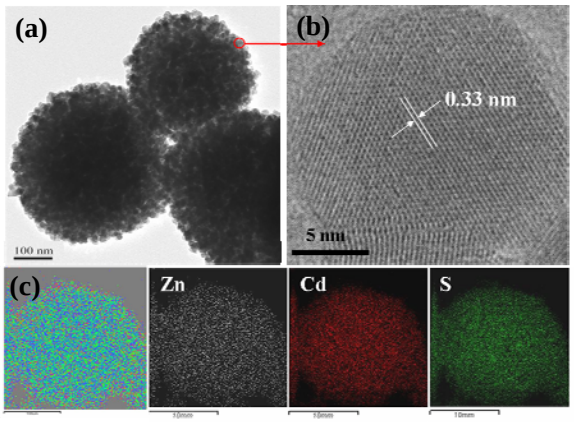

Fig. 3 (a) FESEM, (b) HRTEM and (c) chemical mapping images of $Zn_{0.21}Cd_{0.79}S$ sample.

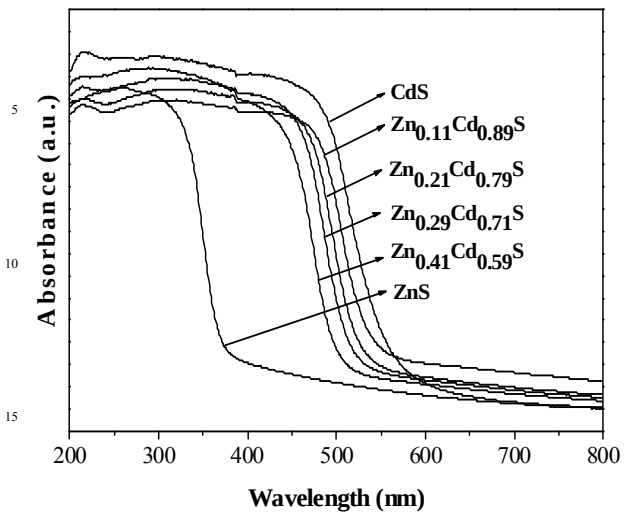

Fig. 4 UV-vis DRS spectra of $Zn_xCd_{1-x}S$ samples.

diameter of about 250 nm, which was formed by uniformly distributed nanoparticles with the average diameter of 14 nm (see HRTEM image), similar to the crystallite size in Table 1. It was ascribed that the fabrication in supercritical hydrothermal conditions without post-thermal treatment could lead to the controllable crystal growth with the small and uniform particle size in addition to the prevention of particle aggregation. The morphologies of ZnS and CdS are also formed by the well-distributed nanoparticles (Fig. S3). The ordered lattice fringes with an inter-planar space of 0.33 nm in $Zn_{0.21}Cd_{0.79}S$ were between (111) ZnS crystal plane (0.31 nm) and (100) CdS plane (0.36 nm) (see HRTEM images in Fig. S3), also implying the formation of solid solution with the volume deformation. The chemical mapping images of $Zn_{0.21}Cd_{0.79}S$ demonstrated that all elements were uniformly distributed in the nanospheres, which was resulted from the stable combination of different atoms in the solid solution.

Typical IV type N_2 adsorption-desorption isotherm of $Zn_{0.21}Cd_{0.79}S$ sample could be found in Fig. S4, corresponding to the worm-like mesoporous structure in the above TEM image. The narrow pore size distribution (insert) at about 10 nm was obviously due to the channel

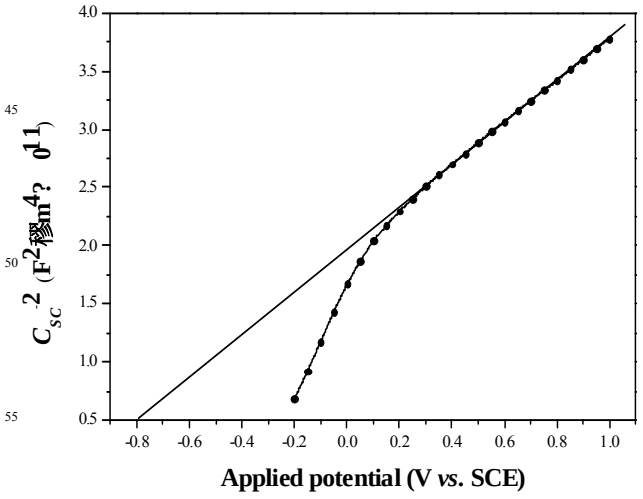

Fig. 5 Mott-Schottky plot for $Zn_{0.21}Cd_{0.79}S$ sample.

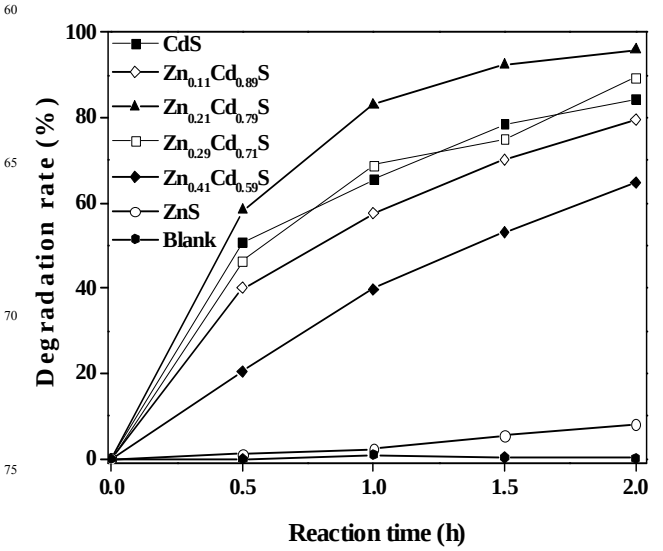

Fig. 6 RhB photocatalytic degradation on different samples. Reaction conditions: 25 mg catalyst, 50 mL 10 mg/L RhB solution, T = 30 °C, $\lambda \geq 420$ nm.

between nanoparticles. The S_{BET}, V_p and D_p of different samples were summarized in Table 1. With the gradually increased X value, the S_{BET} and V_p were enhanced due to the smaller size of Zn atom than that of Cd atom, corresponding to the decreased crystallite size and D_p.

The light absorption properties of $Zn_xCd_{1-x}S$ samples were showed in UV-vis DRS spectra (Fig. 4). With the increase of Zn content, the blue shift of absorption edge led to the gradually weak absorption in visible light region. Correspondingly, E_g of all $Zn_xCd_{1-x}S$ samples summarized in Table 1 were continuously altered from 2.2 eV (CdS) to 3.4 eV (ZnS). Therefore, the compositional control in $Zn_xCd_{1-x}S$ solid solution could adjust the intrinsic E_g and the light absorption was verified more flexibly than that by changing the particle sizes.[40, 41] Variation of E_g with X value in Fig. S5 could be fitted as the quadratic function, $E_g = 0.76\ X^2 + 0.36\ X + 2.23$ ($0 \leq X \leq 1$). The nonlinearity could be attributed that the volume deformation in $Zn_xCd_{1-x}S$ samples altered the band structure and the electronegativity difference of the atoms changed the electrondistribution.[42] The Mott-Schottky plot of $Zn_{0.21}Cd_{0.79}S$ was shown in Figure 5. The positive slope in the linear region possessed a nature of n-type semiconductor for $Zn_{0.21}Cd_{0.79}S$[43], and the flat band potential (E_{fb}) determined by x intercept was -0.8 eV. Therefore, the conduction band potential could be confirmed as -0.9 eV, since the conduction band of n-type semiconductor is very close (0.1 V more negative) to E_{fb}.[30] The valence band potential could be confirmed as 1.4 eV since its band gap was estimated to be 2.3 eV in Table 1. Thus, $Zn_{0.21}Cd_{0.79}S$ could form the $\bullet O_2^-$ based on the negative conduction band than the standard redox potential of $O_2/\bullet O_2^-$ (-0.33 eV *vs* NHE). However, the photo-generated holes could not oxidize OH- to give •OH due to the more negative valence band than the standard redox potential of OH•/OH- (2.38 eV *vs* NHE).[24] At the same time, the lower recombination rate of photo-induced electrons and holes in uniform $Zn_xCd_{1-x}S$ solid solution indicated the more efficient separation of charges which facilitated the photocatalytic reaction, based on the much weaker characteristic PL peak at 757 nm of$Zn_{0.21}Cd_{0.79}S$ than that of ZnS, CdS and 0.21ZnS-0.79CdS(M) sample mechanically mixed with ZnS and CdS (Figure S6). Figure S7 further revealed that the stronger photocurrent density of $Zn_{0.21}Cd_{0.79}S$ than that

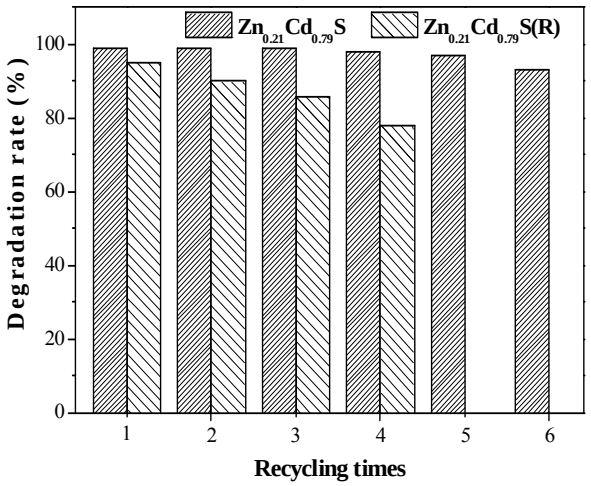

Fig. 7 Recycling test of $Zn_{0.21}Cd_{0.79}S$ and $Zn_{0.21}Cd_{0.79}S$(R) catalysts. Reaction conditions: 25 mg catalyst, 50 mL 10 mg/L RhB solution, $\lambda \geq 420$ nm, $T = 30\,^{\circ}C$, reaction time = 2 h.

of ZnS, which was similar to that of CdS under visible light irradiation although its visible-light absorption was weaker than CdS. It could be attributed that the built-in electric field in solid solution pushed the photo-induced electrons and holes to the opposite sides and then efficiently transported charge carriers through coherent boundaries.[19, 44, 45]

To estimate the photocatalytic performance of $Zn_xCd_{1-x}S$ samples under visible light irradiations ($\lambda \geq 420$ nm), the degradation reaction of RhB and 4-CP was investigated. In Fig. 6, no significant degradation of RhB in the solution could be found without catalysts under visible light irradiations. The activity of $Zn_xCd_{1-x}S$ strongly depended on the tunable composition since the gradual increase of Zn content in $Zn_xCd_{1-x}S$ led to the greatly enhanced degradation of RhB and $Zn_{0.21}Cd_{0.79}S$ exhibited the highest photoactivity. Further enhanced Zn content induced the weaker visible-light harvesting and thus presented the decreased degradation rate, although the S_{BET} increased significantly. Additionally, $Zn_{0.21}Cd_{0.79}S$ also showed the higher activity in comparison to 0.21ZnS-0.79CdS(M) sample (Fig. S8). The high activity of $Zn_{0.21}Cd_{0.79}S$ than other samples could beattributed that the solvothermal process in supercritical fluid induced (1) the strong combination and well-dispersion of different atoms in the $Zn_xCd_{1-x}S$ solid solution, (2) the formation of uniform crystal growth and small particle size without particle aggregation, (3) the high S_{BET} and large pore volume with porous transportation channel between nanoparticles beneficial for the contact of reactant with catalyst, (4) the lower recombination rate of photo-induced electrons and holes in solid solution, realizing the efficient separation of charges and thus facilitating the photocatalytic process. Furthermore, $Zn_{0.21}Cd_{0.79}S$ prepared near the ethanol supercritical point (243 °C and 6.4 MPa) exhibited the higher activity than that at lower or higher temperature, as shown in Fig. S9, implying the supercritical point was beneficial for the uniform crystal growth and the further higher supercritical temperature was harmful for the control of crystallite size. In order to exclude the sensitive effect of RhB during the photocatalytic reaction, degradation of 4-CP was also investigated (Fig. S10). It could be found that $Zn_{0.21}Cd_{0.79}S$ sample still exhibited the highest degradation rate of 4-CP, in accordance with the decomposition of RhB.

As we know, the durability of sulphide was the key and attractive performance for the practical applications due to the problem of photo-corrosion. Fortunately, we found that the improved stability of $Zn_xCd_{1-x}S$ catalyst prepared *via* supercritical solvothermal method, according to Fig. 7. Comparing to $Zn_{0.21}Cd_{0.79}S$(R) sample prepared according to the previous report[25], $Zn_{0.21}Cd_{0.79}S$ showed the stable photocatalytic decomposition of RhB after recycling test for 6 times with little leaching less than 0.6 wt%, based on the ICP result. Meanwhile, the crystallization of catalyst was not changed significantly during the recycling test (see Fig. S11). It was obviously due to the strong interaction between different atoms in $Zn_xCd_{1-x}S$ obtained by supercritical solvothermal route, efficiently inhibiting the oxidation of catalyst and preventing the collapse of porous structure. Meanwhile, the spheric morphology of $Zn_xCd_{1-x}S$ catalysts could realize the easy separation from solution, beneficial for the practical applications.

4. Conclusions

This work developed a novel supercritical solvothermal approach to prepare $Zn_xCd_{1-x}S$ solid solution in uniform nanoparticles with large surface area and large pore volume, corresponding to the high activity in visible-light driven photocatalytic degradation of organic pollutants. More importantly, it displayed excellent durability in photocatalysis owing to the strong stability against either the structural damage or the oxidation. This approach could be further generalized as the large-scale synthesis of other nano-structured materials used in various areas.

ACKNOWLEDGMENTS

This work was supported by National Natural Science Foundation of China (21207091, 21261140333 and 21237003), Program for Changjiang Scholars and Innovative Research Team in University (IRT1269), International Joint Laboratory on Resource Chemistry (IJLRC) and Shanghai Government (11JC1409000).

References

1 X. B. Chen, L. Liu, P. Y. Yu and S. S. Mao, *Science*, 2011, 331, 746-750.
2 X. C. Wang, K. Maeda, A. Thomas, K. Takanabe, Xin, G. J. M. Carlsson, K. Domen and M. Antonietti, *Nature Mater.*, 2009, 8, 76-80.
3 X. F. Chen, X. C. Wang, Y. D. Hou, J. H. Huang, L. Wu and X. Z. Fu, *J. Catal.*, 2008, 255, 59-67.
4 Y. N. Huo, X. L. Yang, J. Zhu and H. X. Li, *Appl. Catal. B*, 2011, 106, 69-75.
5 Y. N. Huo, J. Zhang, M. Miao and Y. Jin, *Appl. Catal. B*, 2012, 111-112, 334-341.
6 L. W. Zhang and Y. F. Zhu, *Catal. Sci. Technol.*, 2012, 2, 694-706.
7 Y. Liu, Y. X. Yu and W. D, Zhang, *J. Phys. Chem. C*, 2013, 117, 12949-12957.
8 X. Zong, H. J. Yan, G. P. Wu, G. J. Ma, F. Y. Wen, L. Wang and C. Li, *J. Am. Chem. Soc.*, 2008, 130, 7176-7177.
9 X. Zong, G. P. Wu, H. J. Yan, G. J. Ma, J. Y. Shi, F. Y. Wen, L. Wang and C. Li, *J. Phys. Chem. C*, 2010, 114, 1963-1968.
10 Y. Liu, Y. X. Yu and W. D. Zhang, *J. Phys. Chem. C*, 2013, 117, 12949-12957.
11 Y. D. Hou, A. B. Laursen, J. S. Zhang, G. G. Zhang, Y. S. Zhu, X. C. Wang, S. Dahl and I. Chorkendorff, *Angew. Chem. Int. Ed.*, 2013, 52, 3621-3625.
12 J. G. Jiang, M. Wang, L. J. Ma, Q. Y. Chen and L. J. Guo, *Inter. J. Hydrogen Energy*, 2013, 38, 13077-13083.

13 N. Soltani, E. Saiona, W. M. M. Yunus, M. Erfani,M. Navasery, G. Bahmanrokh and K. Rezaee, *Appl. Surface Sci.*, 2014, 290, 440-447.
14 J. S. Zhang, M. W. Zhang, R. Q. Sun and X. C. Wang, *Angew. Chem. Int. Ed.*, 2012, 51, 10145-10149.
15 A. T. Nguyen, Y. D. Chiou, W. H. Lin, Y. H. Lu and Y. J. Hsu, *Appl. Catal. B*, 2014, 476, 140-147.
16 L. Wang, X. A. Wang, R. Chen, C. Y. Wu, Y. Q. Yu, J. Xu, J. G. Hu and L. B. Luo, *J. Appl. Phys.*, 2014, 115, 063108.
17 L. J. Chen, J. D. Liao, Y. J. Chuang and Y. S. Fu, *J. Am. Chem. Soc.*, 2011, 133, 3704-3707.
18 M. D. Regulacio and M. Y. Han, 43, *Acc. Chem. Res.*, 2010, 5, 621-630.
19 M. C. Liu, L. Z. Wang, G. Q. Lu, X. D. Yao and L. J. Guo, *Energy Environ. Sci.*, 2011, 4, 1372-1378.
20 L. Lu, Y. Shen, X. Chen, L. Qian and K. Lu, *Science*, 2004, 304, 422-426.
21 T. Hirai, Y. Bando and I. Komasawa, *J. Phys. Chem. B*, 2002, 106, 8967-8970.
22 Y. T. Nien, P. W. Chen and I. G. Chen, *J. Alloys Compd.*, 2008, 462, 398-403.
23 Y. F. Yu, J. Zhang, X. Wu, W. W. Zhao and B. Zhang, *Angew. Chem. Int. Ed.*, 2012, 51, 897-900.
24 W. J. Li, D. Z. Li, W. J. Zhang, Y. Hu, Y. H. He and X. Z. Fu, *J. Phys. Chem. C*, 2010, 114, 2154-2159.
25 W. Z. Wang, W. Zhu and H. L. Xu, *J. Phys. Chem. C*, 2008, 112, 16754-16758.
26 W. J. Li, D. Z. Li, Z. X. Chen, H. J. Huang, M. Sun, Y. H. He and X. Z. Fu, *J. Phys. Chem. C*, 2008, 112, 14943-14947.
27 M. K. Devaraju and I. Honma, *Adv. Energy Mater.*, 2012, 2, 284-297.
28 R. H. Sui and P. Charpentier, *Chem. Rev.*, 2012, 112, 3057-3082.
29 J. A. Darr and M. Poliakoff, *Chem. Rev.*, 1999, 99, 495-541.
30 J. T. Han, Y. H. Huang, X. J. Wu, C. L. Wu, W. Wei, B. Peng, W. Huang and J. B. Goodenough, *Adv. Mater.*, 2006, 18, 2145-2148.
31 A. Sahraneshin, S. Takami, D. Hojo, K. Minami, T. Arita and T. Adschiri, *J. Supercritical Fluids*, 2012, 62, 190-196.
32 T. Adschiri, Y. Hakuta and K. Arai, *Ind. Eng. Chem. Res.*, 2000, 39, 4901-4907.
33 D. M. Kempaiah, D. Rangappa and I. Honma, *Chem. Commun.*, 2012, 48, 2698-2700.
34 G. Aksomaityte, F. Cheng, A. L. Hector, J. R. Hyde, W. Levason, G. Reid, D. C. Smith, J. W. Wilson and W. J. Zhang, *Chem. Mater.*, 2010, 22, 4246-4253.
35 V. Luca, S. Djajanti and R. F. Howe, *J. Phys. Chem. B*, 1998, 102, 10650-10657.
36 R. Ramesham, *Thin Solid Films*, 1998, **322**, 158-166.
37 J. Xu , Y. B. Tang , X. Chen, C. Y. Luan , W. F. Zhang, J. A. Zapien, W. J. Zhang, H. L. Kwong, X. M. Meng, S. T. Lee and C. S. Lee, *Adv. Funct. Mater.*, 2010, 20, 4190-4195.
38 S. N. Garaje, S. K. Apte, S. D. Naik, J. D. Ambekar, R. S. Sonawane, M. V. Kulkarni, A. Vinu and B. B. Kale, *Environ. Sci. Technol.*, 2013, 47, 6664-6672.
39 X. H. Zhong, Y. Y. Feng, W. Knoll and M. Y. Han, *J. Am. Chem. Soc.*, 2003, 125, 13559-13563.
40 J. B. Lu, Y. Dai, M. Guo, W. Wei, Y. D. Ma, S. H. Han and B. B. Huang, *ChemPhysChem.*, 2012, 13, 147-154.
41 J. Wang, B. Huang, Z. Wang, P. Wang, H. Cheng, Z. Zheng, X. Qin, X. Zhang, Y. Dai and M. H. Whangbo, *J. Mater. Chem.*, 2011, 21, 4562-4567.
42 S. H. Wei, S. B. Zhang and A. Zunger, *J. Appl. Phys.*, 2000, 87, 1304-1311.
43 M. T. Li, J. G. Jiang and L. J. Guo, *Inter. J. hydrogen energy*, 2010, 35, 7036-7042.
44 X. Zhao, S. Y. Wei and C. X. Xia, *Physica E*, 2007, 39, 209-213.
45 C. C. Shieh, X. Y. Cui, B. Delley and C. Stampfl, *J. Appl. Phys.*, 2011, 109, 083721.

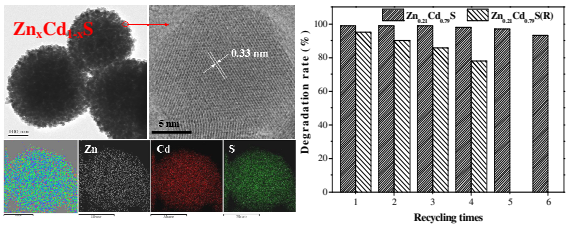

$Zn_xCd_{1-x}S$ solid solution in uniform nanoparticles prepared by supercritical solvothermal route have achieved the high photocatalytic activity and durability.